J MATER SCI 41 (2006) 597–609

Grain boundary sliding revisited: Developments in sliding over four decades

TERENCE G. LANGDON
Departments of Aerospace & Mechanical Engineering and Materials Science, University of Southern California, Los Angeles, CA 90089-1453, USA
E-mail: langdon@usc.edu

It is now recognized that grain boundary sliding (GBS) is often an important mode of deformation in polycrystalline materials. This paper reviews the developments in GBS over the last four decades including the procedures available for estimating the strain contributed by sliding to the total strain, ξ, and the division into Rachinger GBS in conventional creep and Lifshitz GBS in diffusion creep. It is shown that Rachinger GBS occurs under two distinct conditions in conventional creep depending upon whether the grain size, d, is larger or smaller than the equilibrium subgrain size, λ. A unified model is presented leading to separate rate equations for Rachinger GBS in power-law creep and superplasticity. It is demonstrated that these two equations are in excellent agreement with experimental observations. There are additional recent predictions, not fully resolved at the present time, concerning the role of GBS in nanostructured materials. © *2006 Springer Science + Business Media, Inc.*

1. Introduction

Deformation by creep refers to the nonrecoverable plastic strain occurring in a material when it is subjected to a constant stress (or a constant load) over an extended period of time. An interest in creep first developed more than one-hundred years ago with the classic report by Phillips [1] documenting the creep of a wide range of materials from India-rubber to glass and metal wires. This and other early reports, most notably by Andrade [2, 3], set the scene for the extensive investigations of the creep phenomenon which have continued to the present day.

It is now recognized that the creep strains occurring in crystalline materials are due to the presence of defects within the matrix. Three distinct types of defects may be identified: there are point defects (vacancies), line defects (dislocations) and planar defects (grain boundaries). In practice, each type of defect plays a role in determining the creep behavior.

Diffusion creep refers to the flow of vacancies which occurs in a polycrystalline material under the action of an external stress. This flow occurs because the external stress produces an excess of vacancies along those grain boundaries lying perpendicular to the tensile axis and a corresponding depletion of vacancies along those grain boundaries experiencing a compressive stress. Thus, there is a stress-directed flow of vacancies with the flow occurring to restore equilibrium. This mechanism was first suggested by Nabarro [4] and subsequently developed mathematically by Herring [5]. Later, Coble [6] pointed out that vacancy flow may occur also along the grain boundaries. These two processes are now designated Nabarro-Herring and Coble diffusion creep, respectively, and, despite some arguments against the occurrence of these mechanisms [7, 8], it is now generally recognized that the theory of diffusion creep is well-established and the predictions of the models are consistent with microstructural observations including, for example, the occurrence of precipitate-free zones [9, 10].

Dislocations generally play the major role in producing the creep strain in polycrystalline materials, at least under conditions where the strain rates are reasonably rapid. The intragranular movement of dislocations takes place when dislocation loops expand outwards from dislocation sources (such as Frank-Read sources) and the interactions between loops on different slip planes lead to a process in which strain is accrued through a combination of dislocation climb and glide. In simple systems, such as pure metals, the dislocations glide very rapidly on their slip planes and the rate-controlling process is the rate of climb of edge dislocations. It has been shown that creep controlled by climb leads to a power-law relationship in which the strain rate varies with stress raised to an exponent, n, which is close to ~4.5 [11]. However, solute

0022-2461 © *2006 Springer Science + Business Media, Inc.*
DOI: 10.1007/s10853-006-6476-0

atoms may form preferentially around the dislocations in the form of impurity atmospheres in many solid solution alloys and these atmospheres exert a dragging influence on the glide of dislocations so that viscous glide becomes the rate-controlling process in these materials. Under these conditions, it has been shown that the stress exponent is reduced to $n = 3$ [12]. In practice, the situation is often more complex because in alloys there may be a transition with increasing stress from control by climb to control by glide, thereby producing a transition from $n \approx 4.5$ to $n = 3$ [13], and at even higher stresses the dislocations may break away from their solute atmospheres so that $n > 3$ and ultimately, at the highest stresses, climb again becomes the rate-controlling process [14]. The principles of this break-away have been modeled in detail and the predictions show good agreement with experimental data [15].

It is more difficult to assess the role of grain boundaries in creep deformation by comparison with the role of vacancies or dislocations. As a consequence of this complexity, the principles associated with producing creep strain through grain boundary effects have been developed more recently. Furthermore, and as will be demonstrated in this report, there remain some uncertainties with respect to the precise role of grain boundaries in the new and advanced nanostructured materials.

Grain boundary sliding (GBS) denotes the displacement which occurs when, in response to an external stress, two grains slide over each other with the movement taking place at, or in the immediate vicinity of, their mutual interface. The possibility that GBS may occur in a polycrystalline material was first inferred more than ninety years ago by Rosenhain and co-workers [16–18] from qualitative observations of the formation of steps at the grain boundaries of polycrystalline samples during deformation. Subsequently, Moore *et al*. [19, 20] were the first to make use of surface marker lines and to observe, as in many subsequent experiments, the development of sharp offsets on the surface of a Pb-2% Sn alloy at the points where the lines intersected the grain boundaries. The first demonstration of GBS in bi-crystals was reported in 1948 using Sn and a testing temperature only a few degrees below the melting temperature [21]. Following this early work, there were several reports of GBS in bi-crystals using, for example, Al [22, 23], Cu [24], Sn [25] and Zn [26].

These early reports provide information on the limited details of GBS that were available at the time when the *Journal of Materials Science* was introduced as a scientific publication in 1966. Two early papers will serve to demonstrate the level of understanding at that time. A report entitled "An Investigation of Grain Boundary Sliding during Creep," published in volume 2, described experimental measurements of GBS in a Mg-0.78 wt% Al alloy and showed that GBS may make a significant contribution to the overall strain in creep testing at low stress levels [27]. A later report entitled "The Dependence of Grain Boundary Sliding on Shear Stress," published in volume 3, showed that the sliding offsets measured experimentally were proportional, for four different metals, to the shear component of the applied stress resolved in the boundary plane [28]. These papers provided some of the earliest information on the occurrence of GBS in polycrystalline metals and it is now appropriate in the present paper, published four decades later, to re-examine the role of GBS in terms of the many developments that have taken place over the last forty years. For convenience, a more formal definition of GBS is presented in the following section and the subsequent sections describe the recent developments that have led to the current understanding of creep flow by GBS.

2. Formal definitions of GBS

It is now recognized that there are two separate, and mechanistically distinct, types of GBS.

The first type of GBS refers to the relative displacement of adjacent grains where the grains retain essentially their original shape but they become visibly displaced with respect to each other. This type of GBS is designated *Rachinger sliding* [29] and it occurs in a polycrystalline matrix under creep conditions where there is a net increase in the number of grains lying within the gauge length along the direction of the tensile stress. In practice, grains have irregular shapes in polycrystalline matrices and it follows, therefore, that Rachinger sliding must be accommodated by some intragranular movement of dislocations within the adjacent grains.

The second type of GBS occurs exclusively in Nabarro-Herring and Coble diffusion creep and it refers to the boundary offsets that develop as a direct consequence of the stress-directed diffusion of vacancies. This type of GBS is designated *Lifshitz sliding* [30] and it is illustrated schematically in Fig. 1. Three adjacent grains are shown at zero strain in Fig. 1a where the tensile axis is vertical and two marker lines are scribed parallel to the stress axis at AA′ and BB′, respectively. Under conditions of Nabarro-Herring or Coble diffusion creep, vacancies diffuse from the transverse to the longitudinal boundaries where this is equivalent to the removal of layers of atoms from the longitudinal boundaries and the plating of these atoms along the transverse boundaries. Thus, as shown in Fig. 1b, the two marker lines remain unchanged in the lower grain but they move closer together in the two upper grains as material is removed from the central boundary. The occurrence of diffusion creep leads, therefore, to offsets in the marker lines as shown in Fig. 1b and it follows that for Lifshitz sliding there is no net increase in the number

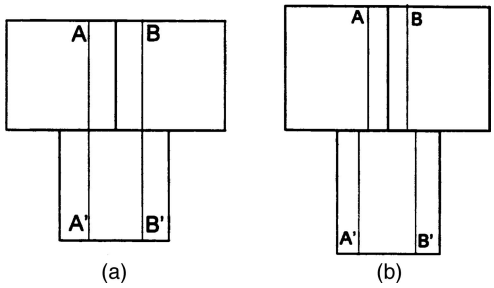

Figure 1 The occurrence of Lifshitz GBS in diffusion creep for an array of three grains: the tensile axis is vertical, AA′ and BB′ are marker lines and the grains are shown (a) before creep and (b) after creep testing.

of grains measured within the gauge length parallel to the tensile stress.

The processes of Rachinger GBS and Lifshitz GBS are mechanistically different because Rachinger sliding requires accommodation by intragranular slip whereas Lifshitz sliding is itself an accommodation process for conventional diffusion creep. Nevertheless, despite this clear distinction, both processes produce similar offsets in marker lines at the grain boundaries. Thus, it follows that care must be taken to distinguish clearly and unambiguously between these two deformation processes. This can be done by noting, for example, that the grains retain essentially their original shapes in Rachinger sliding but they become elongated along the tensile axis in Lifshitz sliding. In the following sections, all references to GBS denote Rachinger sliding except only when Lifshitz sliding is specifically described with reference to diffusion creep.

3. Estimating the contribution of GBS to the overall strain

Many efforts have been devoted over the years to producing reliable and reproducible procedures for estimating the contribution of GBS to the total strain. The total strain achieved under creep conditions, ε_t, may be expressed in a rigorous form as:

$$\varepsilon_t = \varepsilon_g + \varepsilon_{\text{gbs}} + \varepsilon_{\text{dc}} \tag{1}$$

where ε_g is the strain associated with intragranular dislocation processes within the grains, ε_{gbs} is the strain due to Rachinger GBS including the associated accommodation through intragranular slip and ε_{dc} is the strain due to diffusion creep including Lifshitz GBS. In practice, creep experiments are often conducted under testing conditions where there is a negligible contribution from diffusion creep and Equation 1 reduces to the more convenient form of

$$\varepsilon_t = \varepsilon_g + \varepsilon_{\text{gbs}} \tag{2}$$

The contribution of GBS to the total strain, ξ, is then expressed as

$$\xi = \frac{\varepsilon_{\text{gbs}}}{\varepsilon_t} \tag{3}$$

In order to obtain a meaningful measure of ξ, it is first recognized that the occurrence of GBS will lead, at any selected boundary, to the occurrence of offsets in three mutually perpendicular directions. This situation is illustrated schematically in Fig. 2 where there are three orthogonal displacements, u, v and w, due to the occurrence of GBS between grains 1 and 2 under the action of an applied stress, σ. Fig. 2 shows also the sliding vector in the grain boundary plane, S, and two angles that serve to define the boundary orientation with respect to the tensile axis: there is an angle θ between the trace of the boundary on the upper exposed surface and the tensile axis and there is an additional angle ψ between the tensile axis and the trace of the boundary on a polished surface cut perpendicular to the upper surface. The sliding contribution, ξ, may be estimated by determining the value of ε_{gbs} from individual measurements of one or more of these three separate displacements.

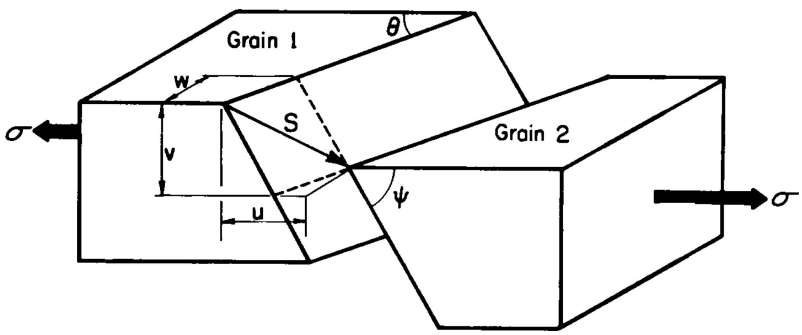

Figure 2 The occurrence of three sliding offsets, u, v and w, when GBS occurs between grains 1 and 2 under the action of an applied stress, σ: S denotes the sliding vector.

It follows from first principles that the individual sliding displacements shown in Fig. 2 are related through the expression

$$u = \frac{v}{\tan\psi} + \frac{w}{\tan\theta} \tag{4}$$

However, it is impractical to use Equation 4 in experimental measurements of ξ because of the difficulties of measuring the angles θ and ψ at every boundary. It is necessary therefore to develop more simplified procedures.

If longitudinal marker lines are scribed on the specimen surface prior to creep testing, it is possible to take individual measurements of u along selected lines at all points where the marker lines intersect the grain boundaries. It follows that the sliding strain is then given by [31]

$$\varepsilon_{\text{gbs}} = n_\ell \bar{u}_\ell \tag{5}$$

where n is the number of grains per unit length, $\bar{u}$ is the average value of u and the subscript ℓ denotes taking measurements along a longitudinal line parallel to the tensile axis.

Inspection of Fig. 2 shows that it is not easy in practice to take measurements of u along a longitudinal traverse but it is relatively easy to use longitudinal markers to take measurements of the sliding offset w. For this condition, the sliding strain is given by [31]

$$\varepsilon_{\text{gbs}} = k' n_\ell \bar{w}_\ell \tag{6}$$

where $\bar{w}$ is the average value of w, k' is a constant and ℓ again denotes taking measurements along a longitudinal traverse. The value of k' was estimated theoretically as ~1.62 and determined experimentally as ~1.44 [31]. Based on these results, it was proposed that Equation 6 may be used to measure the sliding contribution with a value of $k' \approx 1.5$ [32].

An alternative procedure is to scribe transverse marker lines perpendicular to the tensile axis and to record measurements of u and the angle θ at every boundary intersected by the line [33]. Fig. 3 shows an example of the very clear offsets occurring in a transverse marker line for a Mg-0.78% Al alloy strained to 2.49% at a temperature of 473 K under an applied stress of 17.2 MPa: the tensile axis is horizontal [27]. For this condition, the sliding strain is given by [31]

$$\varepsilon_{\text{gbs}} = n_t \overline{(u \tan\theta)}_t \tag{7}$$

where t denotes the procedure of taking measurements along a transverse traverse.

An alternative, and easier, experimental procedure is to take measurements of the vertical offset v perpendicular to the specimen surface using interferometry. An example of the offsets revealed by interferometry is shown in Fig. 4 for a Mg-0.78% Al alloy pulled to an elongation of 1.5% at 473 K under a stress of 27.6 MPa [34]. It is apparent that the fringes in Fig. 4 run essentially from left to right but there are clear discontinuities in the dark central fringes at the points where they intersect the grain boundaries. In addition, the fringes are continuous along the exposed facet of the boundary between the two central grains. These fringes have a separation of 0.27 μm and, since the discontinuities at the boundaries in Fig. 4 are of the order of one fringe displacement, it follows that the value of v perpendicular to the specimen surface is ~0.3 μm. By using an interference microscope, it is fairly easy to rotate the fringes so that they lie approximately perpendicular to each separate grain boundary within any field of view and to take individual measurements of the v offsets. For this condition,

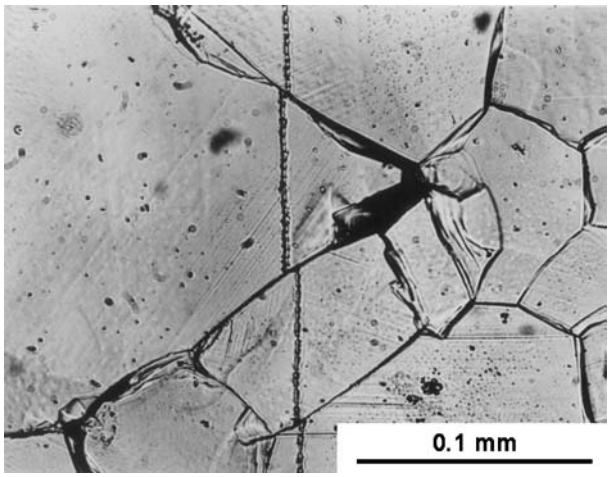

Figure 3 The occurrence of GBS revealed by the boundary offsets in a transverse marker line for a Mg-0.78% Al alloy tested under creep conditions at 473 K: the tensile axis is horizontal [27].

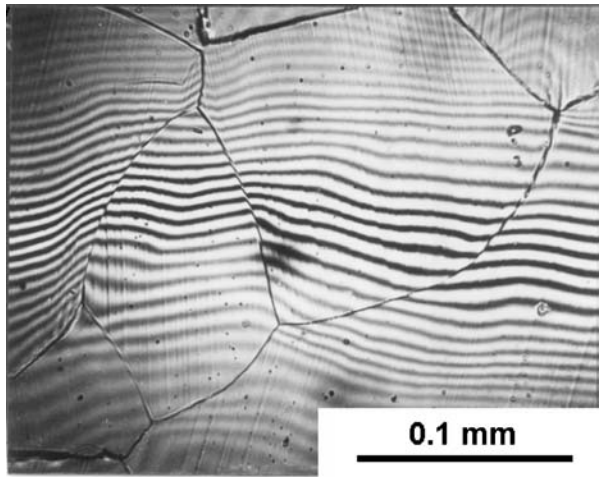

Figure 4 The occurrence of GBS revealed by interferometry for a Mg-0.78% Al alloy tested under creep conditions at 473 K [34].

the sliding strain is given by [32]

$$\varepsilon_{\text{gbs}} = k'' n_r \bar{v}_r \tag{8}$$

where k'' is a constant, $\bar{v}$ is the average value of the v measurements and the subscript r denotes the procedure of taking measurements at randomly selected boundaries. In practice, the value of k'' depends upon whether the surface of the specimen is "polished" so that the internal boundaries intersect the free surface at random angles or "annealed" so that the internal boundaries intersect the free surface at angles closer to 90°. Experiments show the values of k'' are ~1.1 for polished surfaces and ~1.5 for annealed surfaces [35].

There appears in principle to be an alternative procedure for determining ε_{gbs} by taking measurements of the grain shapes and using these values for a direct determination of the magnitude of the intragranular strain, ε_g, and hence the strain due to sliding through Equation 2. In practice, however, it was shown using regular grids printed onto the surfaces of creep specimens that measurements of grain shape lead to an underestimation of ε_g, and hence an overestimation of ε_{gbs}, because the boundaries tend to migrate during creep in order to maintain a reasonably equiaxed grain configuration [35]. Accordingly, it is concluded that any determination of ε_{gbs} requires direct measurements of the offsets produced at grain boundaries as depicted in Fig. 2. Equations 5–8 are available for use in experimental investigations and for subsequent estimates of the magnitudes of ξ using Equation 3.

4. Developing a rate equation for GBS

A comprehensive approach was developed several years ago for interpreting the creep behavior of crystalline materials [36]. In this approach, the behavior is quantified in terms of the strain rate in the secondary or steady-state stage of creep through the dependence of this rate on experimental parameters such as the applied stress, σ, the absolute temperature, T, and the grain size of the material, d.

It is convenient to express the steady-state creep rate, $\dot{\varepsilon}$, by a relationship of the form

$$\dot{\varepsilon} = \frac{ADG\mathbf{b}}{kT}\left(\frac{\mathbf{b}}{d}\right)^p\left(\frac{\sigma}{G}\right)^n \tag{9}$$

where D is the diffusion coefficient ($=D_o \exp(-Q/RT)$, where D_o is a frequency factor, Q is the appropriate activation energy for the diffusive process and R is the gas constant), G is the value of the shear modulus at the testing temperature, $\mathbf{b}$ is the Burgers vector, k is Boltzmann's constant, p and n are constants defined as the inverse grain size exponent and the stress exponent, respectively, and A is a dimensionless constant.

Inspection of Equation 9 shows that the creep rate may be defined uniquely in terms of the values predicted for the four parameters Q, p, n and A. In practice, however, the value of the dimensionless constant A is related to structural features in the material such as the stacking-fault energy or the presence of precipitates and it is more convenient to compare the various creep mechanisms in terms of the values predicted for Q, p and n. Thus, the theories for diffusion creep predict $n = 1$ with $p = 2$ and $D = D_\ell$ for Nabarro-Herring creep [4, 5] and with $p = 3$ and $D = D_{\text{gb}}$ for Coble creep [6] where D_ℓ and D_{gb} are the coefficients for lattice and grain boundary diffusion, respectively. Similarly, the theoretical equations for control by dislocation climb and dislocation glide require $n \approx 4.5$, $p = 0$ and $D = D_\ell$ [11] and $n = 3$, $p = 0$ and $D = \tilde{D}$ [12], respectively, where $\tilde{D}$ is the coefficient for inter-diffusion of the solute atoms. It is important, therefore, to develop a similar relationship for the strain rate due to GBS.

An early attempt was made to develop a model for GBS in which sliding occurred through the movement of dislocations along, or adjacent to, the grain boundaries through a combination of climb and glide [37] and this model led to a relationship of the form given in Equation 9 with $n = 2$, $p = 1$ and $D = D_\ell$. Since this model has a stress exponent of 2 whereas intragranular dislocation mechanisms have values of $n \geq 3$, it follows that the model predicts correctly the increasing importance of GBS at the lower stress levels. Nevertheless, the model is not fully consistent with the experimental situation because it fails to incorporate the occurrence of intragranular slip which is necessary in order to accommodate Rachinger GBS. An alternative approach incorporating accommodation by intragranular slip is described in detail in Section 9.

5. The significance of GBS in ceramics

There is a considerable current interest in the creep of ionic solids because of the potential use of many of these materials in a wide range of high-temperature applications. A review of the literature shows, however, that many of the early creep experiments led to an essentially linear relationship between the steady-state creep rate and the applied stress [38, 39] thereby suggesting that these materials deform predominantly by Nabarro-Herring or Coble diffusion creep. It was shown in later experiments that many ceramic materials also exhibit stress exponents of $n \approx 3 - 5$ at the faster creep rates [40, 41] and under these conditions the measured creep rates are independent of the grain size over a range of grain sizes exceeding one order of magnitude [42]. These results suggest, therefore, that the creep properties of ceramics, including the rate-controlling flow mechanisms, may be interpreted using similar methods to those established for metals. In ad-

dition, there is a similarity between the magnitudes of the intragranular dislocation densities and the sizes of the subgrains formed in ceramics and metals in the region of power-law creep [43, 44]. The only significant exception to the similarity between the creep of ceramics and metals lies in the occurrence of ambipolar diffusion in the diffusion creep of ceramics where, although both the cations and the anions participate in the diffusion process, the two atomic species may diffuse along different paths [45, 46].

The procedures outlined in Section 3 for estimating the values of ξ, where ε_{gbs} is determined from the offsets developed at grain boundaries under creep conditions, are equally applicable to ceramic materials [47]. Furthermore, these methods have been used successfully with several ceramics including MgO [48] and Al_2O_3 [49] where the values of ξ were estimated from measurements of the v offsets. The same experimental methods have been used also for determinations of ξ in geological materials such as $CaCO_3$ [50].

6. The role of GBS in diffusion creep

As noted in Section 2, Lifshitz sliding is an important characteristic of diffusion creep. Furthermore, the boundary offsets produced by Lifshitz sliding are similar in appearance to those produced by Rachinger sliding and, accordingly, the same equations can be used to estimate the contribution of Lifshitz sliding to the total strain.

Fig. 5 shows an example of the appearance of a Magnox ZR55 (Mg-0.55% Zr) alloy after diffusion creep to a strain of 13.3%: this sample had an initial grain size of ~80 μm, it was tested at 673 K under conditions associated with Nabarro-Herring diffusion creep using a constant stress of 2.0 MPa and the tensile axis is vertical [51]. Furthermore, the creep behavior of this specimen was subjected to very extensive analysis to establish unambiguously the occurrence of Nabarro-Herring creep [51, 52]. It is apparent also from Fig. 5 that this alloy is especially useful for sliding measurements because it contains hydride stringers lying parallel to the tensile axis and these stringers may be used for a direct measure of the w sliding offsets. Measurements of these offsets led to an estimate of $\xi \approx 60\%$ under conditions of Nabarro-Herring creep [53] and subsequently there were other reports of sliding measurements in diffusion creep with values of ξ of ~50% in a Mg-0.62% Mn alloy [54] and ~51% in a Mg-0.55% Zr alloy [55]. All of these measurements are mutually consistent and they suggest a contribution from Lifshitz GBS of $\xi \approx 50$–60% in Nabarro-Herring diffusion creep.

It has been shown that the contribution of Lifshitz sliding to the overall strain in diffusion creep may vary in the range from 0 to 100% depending only upon the precise definitions of the strains associated with Lifshitz sliding and the grain elongation due to vacancy flow [56]. This approach is therefore consistent with other more recent analyses [57, 58] but it is inconsistent with an alternative recent analysis predicting a fixed sliding contribution of $\xi \approx 60\%$ in diffusion creep [59].

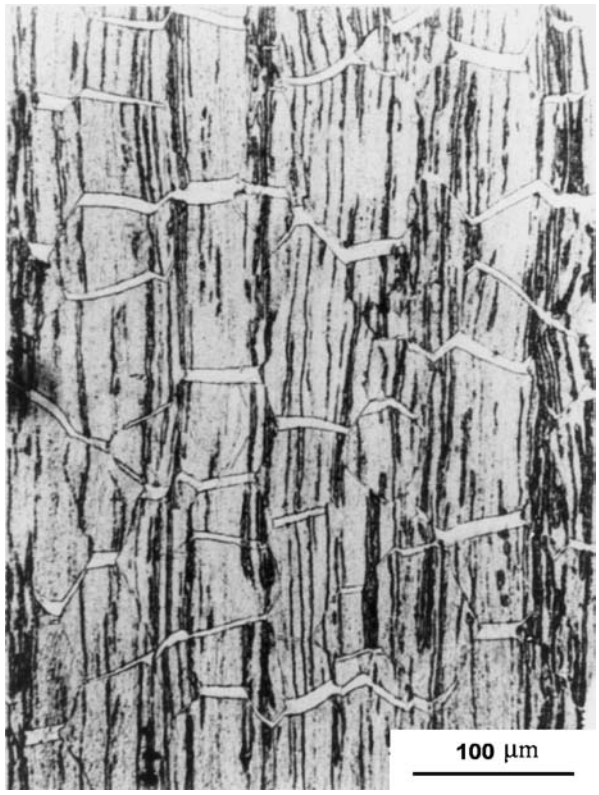

Figure 5 The occurrence of Lifshitz GBS revealed by offsets in hydride stringers in a Mg-0.55% Zr alloy tested under conditions where the strain is due to Nabarro-Herring diffusion creep: the tensile axis is vertical [51].

7. The significance of GBS in superplasticity

Superplasticity refers to the ability of some materials to pull out to very high tensile elongations without fracture. It is now known that there are two fundamental requirements for achieving superplastic flow: (1) a very small and stable grain size, typically <10 μm, and (2) a high testing temperature, typically at least ~0.5 T_m where T_m is the absolute melting temperature of the material [60].

Fig. 6 shows experimental results reported for the superplastic Zn-22% Al eutectoid alloy having a grain size of 2.5 μm [61] where the lower three curves show the variation of the flow stress, σ, with the strain rate, $\dot{\varepsilon}$, for testing temperatures from 423 to 503 K and the upper three curves show the measured elongations to failure, $\Delta L/L_o\%$, for each separate specimen, where ΔL is the total increase in length at the point of fracture and L_o is the initial gauge length. It is apparent that the variation of the flow stress with the strain rate follows a sigmoidal relationship dividing the curve into three separate regimes designated I, II and III. Superplastic elongations are achieved in region II with maximum elongations to

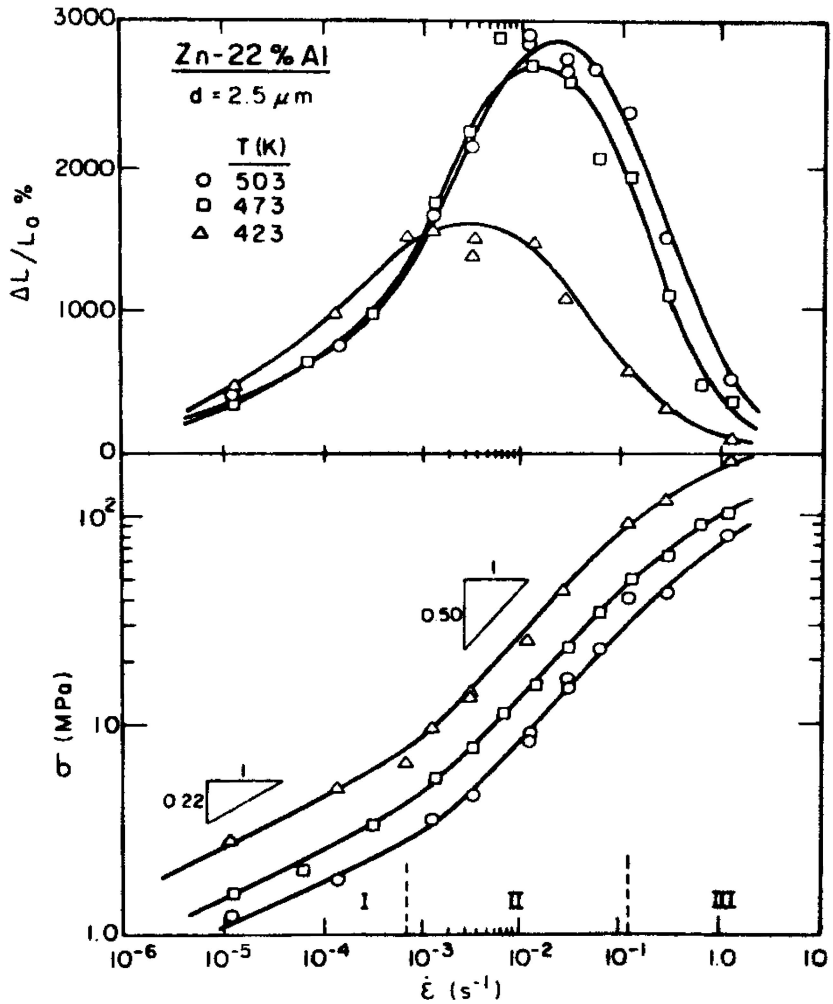

Figure 6 Variation of the elongation to failure (upper) and the flow stress (lower) for the Zn-22% Al eutectoid alloy tested at three different temperatures: superplastic elongations are achieved in region II [61].

failure up to >2000% but there are decreases in the elongations to failure at both slower and faster strain rates in regions I and III, respectively. The strain rate sensitivity, m, defined as the slope of the plot of stress versus strain rate, varies from ~0.5 in the intermediate superplastic region II to ~0.2 in regions I and III. It is now recognized that region III represents conventional creep behavior controlled by an intragranular dislocation creep mechanism whereas extensive experiments have shown that region I is associated with the presence of impurities in the grain boundaries such that this region may be eliminated when using materials of exceptionally high purity [62–64].

Microstructural observations have shown that the grains remain reasonably equiaxed in superplastic flow even when the specimens pull out to very high elongations [65]. This suggests that Rachinger GBS plays an important role in superplasticity so that the grains slide over each other without becoming elongated along the tensile axis. The various equations delineated in Section 3 may be used to estimate the values of the sliding contributions in superplastic flow and there are various reports of the use of these relationships for a wide range of materials [66, 67]. Generally, measurements of this type lead to values of $\xi \approx 50$–70% in the superplastic region II but with significantly lower values recorded for ξ in regions I and III. Thus, the results suggest that GBS makes an important contribution to the overall strain in superplasticity but there appears to be an additional "missing strain" of ~30–50%.

In order to investigate the possibility of a missing strain in the superplastic region II, it was necessary to perform a careful examination of the procedures adopted for estimating the values of ε_{gbs} in superplastic materials [68]. A review of the relevant superplastic literature showed that, without exception, all of the values reported for ε_{gbs}, and thus of ξ, were obtained from measurements of the w offsets along longitudinal marker lines and through the use of Equation 6. Although there were some minor differences in the values used for the constant k' in Equation 6, nevertheless it was concluded that these differences were

essentially insignificant. It was shown instead through a detailed analysis that Equation 6 breaks down when the sliding contribution is very high. There are two reasons for this breakdown. First, very large offsets cannot be measured using this technique since the marker line no longer impinges on a single boundary. Second, there is an accommodation of the grain movement around the edges of each grain and this introduces a specific limitation on the magnitude of each sliding offset. It followed from this analysis that the reported sliding contributions of $\xi \approx 45$–70% in the superplastic region II correspond essentially to a situation where all of the strain is achieved through grain boundary sliding and there is no additional "missing strain" [68].

There are two features of GBS in superplasticity that are different from GBS in conventional creep testing. First, many of the superplastic alloys have two-phase eutectic or eutectoid structures and this raises the possibility of measuring the magnitudes of the sliding offsets on the different types of interfaces. Experiments on the Pb-62% Sn eutectic alloy showed that the largest offsets occur on the Sn-Sn intercrystalline boundaries, there are smaller offsets on the Pb-Sn interphase boundaries and little or no sliding occurs at the Pb-Pb intercrystalline boundaries [69]. Later work on the Zn-22% Al eutectoid alloy showed maximum sliding on the Zn-Zn intercrystalline boundaries, less sliding on the Zn-Al interphase boundaries and a minimum sliding on the Al-Al intercrystalline boundaries [70]. The experimental results for both the Pn-62% Sn and the Zn-22% Al alloys are consistent with the expectation that maximum GBS occurs on the interfaces having the highest values of δD_{gb}, where δ is the grain boundary width [70]. Second, the tensile elongations achieved in superplasticity are very high, often up to and exceeding 1000%, but the equations documented in Section 3 represent viable procedures only when they are used at relatively small elongations. An attempt was made to measure the sliding contribution at an elongation of 100% in the Zn-22% Al eutectoid alloy but this led to an unrealistically low value of $\xi < 20\%$ because of the obvious limitation inherent in the sampling procedure [70]. Accordingly, experiments were conducted to overcome this problem by performing tests on the Zn-22% Al alloy where the magnitude of ξ was measured both at an elongation of ~35% and, after repolishing the samples and scribing new marker lines at an elongation of ~200%, at a total elongation of ~235% [71]. By conducting the experiment in this way, where new polished surfaces and new markers were generated at a high strain, it was demonstrated that there was no diminution in the role of GBS at high elongations. It was therefore concluded that measurements of ξ in the early stages of deformation provide meaningful information on the flow behavior at the much higher superplastic elongations [71].

To obtain more information on the nature of the rate-controlling flow process in superplasticity, the experimental data shown in Fig. 6 may be plotted, for a selected temperature of 503 K, in the form of a deformation mechanism map as shown in Fig. 7 where the normalized grain size, $d/\mathbf{b}$, is plotted against the normalized shear stress, τ/G, where τ is the shear stress: Fig. 7 includes the measured experimental data appropriate to regions I, II and III and, in addition, the theoretical predictions for the re-

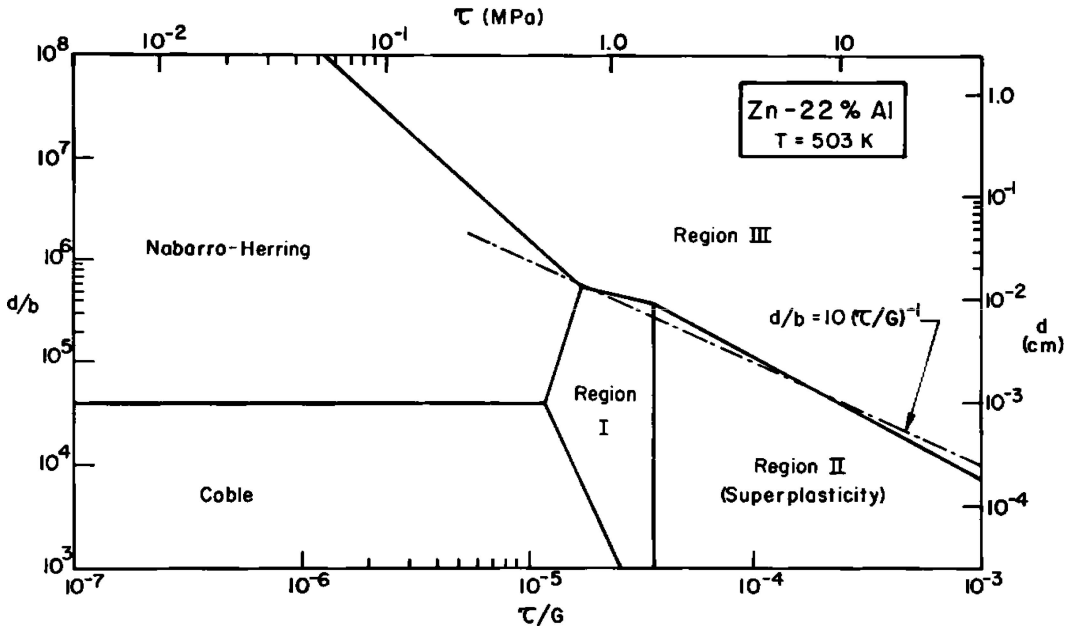

Figure 7 Deformation mechanism map of normalized grain size against normalized shear stress using the experimental data for the Zn-22% Al alloy at 503 K shown in Fig. 6 and the theoretical predictions for Nabarro-Herring and Coble diffusion creep: the broken line shows the condition where the grain size, d, is equal to the subgrain size, λ [72].

gions of Nabarro-Herring and Coble diffusion creep [72]. It is apparent from this map that, at the higher values of τ/G, there is a transition with decreasing grain size from conventional intragranular dislocation creep in region III to superplasticity in region II. It is well established in conventional creep that subgrains are formed within the grains during creep deformation and the average size of these subgrains, λ, is dependent upon the applied stress through a relationship of the form

$$\frac{\lambda}{\mathbf{b}} = \zeta \left(\frac{\tau}{G}\right)^{-1} \tag{10}$$

where ζ is a constant having a value close to ~10 for both metals [36] and ceramics [44]. The broken line superimposed in Fig. 7 represents Equation 10 when the grain size, d, is placed equal to the subgrain size, λ. It is apparent that this line is in excellent agreement with the experimental boundary marking the transition from region III to region II, thereby indicating that superplasticity requires a grain size that is sufficiently small that no subgrains are formed during the deformation process.

8. The rate equations for GBS in creep and superplasticity

The preceding section shows that GBS occurs in polycrystalline solids under two distinct conditions. First, as a separate mechanism contributing to the overall flow of a polycrystal under conditions of high temperature creep, where this is equivalent to flow within region III in the deformation mechanism map shown in Fig. 7. This behavior is characterized by the relationship shown earlier in Equations 1 and 2. Second, when the grain size is very small so that $d \leq \lambda$, GBS represents all of the strain in superplastic flow and deformation occurs in region II in Fig. 7. In order to achieve an understanding of GBS at all grain sizes, it is therefore necessary to determine the rate equation for GBS under both of these conditions.

For superplastic deformation, the nature of the rate equation has been determined in numerous experimental studies. Although there are some very minor variations in the results reported to date, these investigations generally lead to a stress exponent of $n \approx 2$, a value for the exponent of the inverse grain size of $p \approx 2$ and an activation energy close to the value for grain boundary diffusion so that the appropriate diffusion coefficient is D_{gb} [73–76]. Thus, the rate equation for GBS for the condition where $d < \lambda$ is given by

$$\dot{\varepsilon}_{gbs(d<\lambda)} = \frac{A' D_{gb} G \mathbf{b}}{kT} \left(\frac{\mathbf{b}}{d}\right)^2 \left(\frac{\sigma}{G}\right)^2 \tag{11}$$

where A' is a dimensionless constant having an experimental value close to ~10.

A more detailed analysis is required to obtain the rate equation for GBS when $d > \lambda$ because sliding no longer represents all of the creep deformation but rather it occurs as a creep mechanism that contributes an incremental strain to the material. The form of the relationship for this condition was derived using data obtained with high purity (99.995%) aluminum where creep tests were conducted in tension under conditions of constant stress over a range of temperatures from 573 to 773 K and with grain sizes from 200 to 4000 μm [77]. It is important to note also that the creep tests were performed under conditions where diffusion creep made no significant contribution to the overall strain so that the total strain was accurately represented by Equation 2. The values of ξ were determined from extensive measurements of the v sliding offsets using interferometry with the values of ε_{gbs} estimated from Equation 8.

In the absence of any significant contribution from diffusion creep, it follows from Equation 2 that

$$\left(\frac{1}{\xi} - 1\right) = \frac{\varepsilon_g}{\varepsilon_{gbs}} = \frac{\dot{\varepsilon}_g}{\dot{\varepsilon}_{gbs}} \tag{12}$$

Anticipating that the rate equations for intragranular slip and Rachinger GBS are both of the form given in Equation 9, and using the subscripts g and gbs to denote the terms associated with intragranular deformation and GBS, respectively, it follows that Equation 12 may be

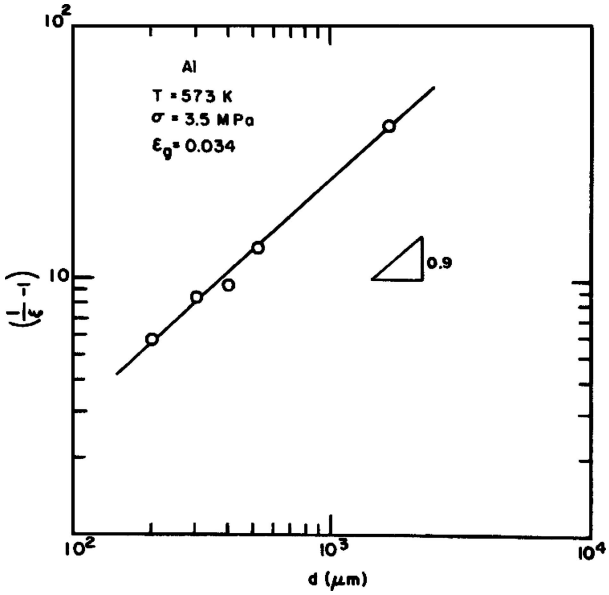

Figure 8 Procedure for estimating the exponent of the inverse grain size for Rachinger GBS, p_{gbs} [77].

re-written in the more explicit form of

$$\left(\frac{1}{\xi}-1\right)=\left(\frac{A_g}{A_{\text{gbs}}}\right)\left(\frac{d}{\mathbf{b}}\right)^{p_{\text{gbs}}-p_g}\left(\frac{\sigma}{G}\right)^{n_g-n_{\text{gbs}}}\left(\frac{D_g}{D_{\text{gbs}}}\right) \tag{13}$$

From creep experiments on pure Al with large grain sizes, under conditions where there was negligible GBS and negligible diffusion creep, it was determined that $n_g \approx 4.5$, $p_g = 0$ and $Q_g \approx 145$ kJ mol^{-1}, where Q_g is the appropriate activation energy for intragranular deformation [78]. These values are consistent with tabulated creep data for polycrystalline and single crystal Al [36] and the measured activation energy is very close to the value of 143.4 kJ mol^{-1} for lattice self-diffusion in pure Al [79].

Specimens having different grain sizes were tested in creep under the same conditions of temperature (573 K) and stress (3.5 MPa) and for the same total time to an identical intragranular strain of $\varepsilon_g = 0.034$. Using Equation 13 with $p_g = 0$, the experimental data were plotted as shown in Fig. 8 to give an exponent of the inverse grain size for Rachinger GBS of $p_{\text{gbs}} \approx 0.9 \pm 0.1$. Additional experiments were conducted at different stresses at a temperature of 573 K using specimens having a grain size of $d \approx 300$ μm and with each specimen taken to an identical total strain of $\varepsilon = 0.02$. These results are plotted in Fig. 9 with $n_g = 4.5$ and $p_{\text{gbs}} = 0.9$ to give a stress exponent for

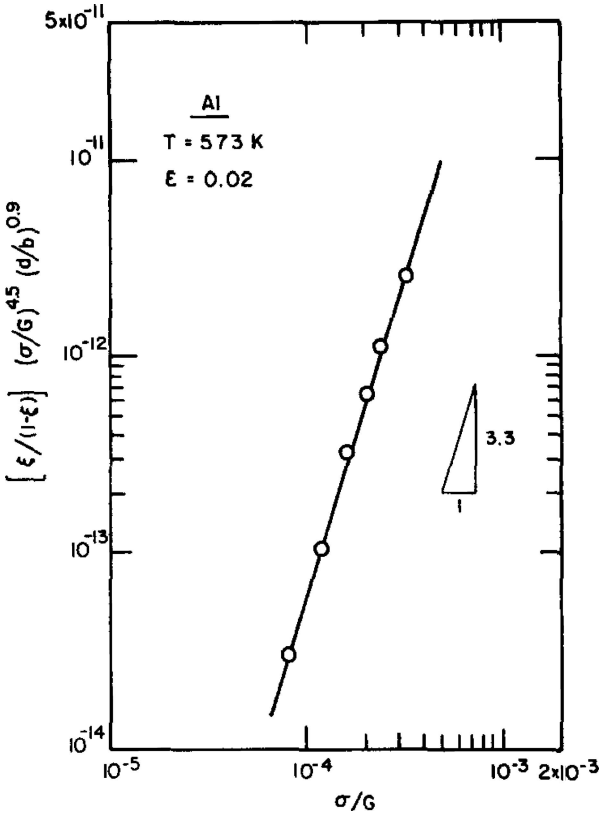

Figure 9 Procedure for estimating the stress exponent for Rachinger GBS, n_{gbs} [77].

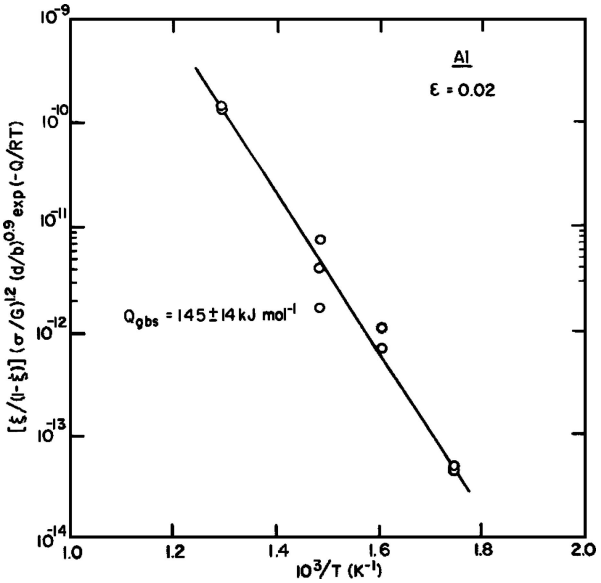

Figure 10 Procedure for estimating the activation energy for Rachinger GBS, Q_{gbs} [77].

Rachinger GBS of $n_{\text{gbs}} \approx 3.3 \pm 0.2$. Finally, specimens with a grain size of ~600 μm were tested at different stresses to a constant total strain of $\varepsilon = 0.02$ and with the tests conducted at different temperatures in the range from 573 to 773 K. These data are plotted in Fig. 10 using Equation 13 with a stress exponent of $n_g - n_{\text{gbs}} = 4.5 - 3.3 = 1.2$, an exponent of the inverse grain size of $p_{\text{gbs}} = 0.9$ since $p_g = 0$ and with an activation energy, Q, equal to the value for lattice self-diffusion (143.4 kJ mol^{-1}). From this plot, the activation energy for Rachinger GBS was estimated as $Q_{\text{gbs}} \approx 145 \pm 14$ kJ mol^{-1}.

It follows from these experiments that the strain rate for Rachinger GBS in power-law creep has a stress exponent of $n_{\text{gbs}} \approx 3$, an exponent for the inverse grain size of $p_{\text{gbs}} \approx 1$ and an activation energy similar to the value for lattice self-diffusion so that the temperature dependence may be incorporated into the rate equation through the value of D_ℓ. Thus, the strain rate for Rachinger GBS occurring under conditions where the grain size is larger than the sub-grain size is given by a relationship of the form [77]

$$\dot{\varepsilon}_{\text{gbs}(d>\lambda)} = \frac{A'' D_\ell G \mathbf{b}}{kT}\left(\frac{\mathbf{b}}{d}\right)\left(\frac{\sigma}{G}\right)^3 \tag{14}$$

where A'' is a dimensionless constant.

9. A unified model for GBS in creep and superplasticity

The preceding section shows there are two separate and distinct relationships for Rachinger GBS. When the grain size is large in conventional creep, the rate of sliding is given by Equation 14; whereas when the grain size is

smaller than the equilibrium subgrain size, no subgrains are formed, flow occurs by superplasticity and the rate of sliding is given by Equation 11. A unified approach is therefore needed to account for these two separate relationships [77].

It is reasonable to assume that Rachinger GBS occurs in an essentially similar way in both creep and superplasticity. Furthermore, there are experimental results showing that the total amount of sliding varies from point to point along any selected grain boundary [80], thereby suggesting that Rachinger sliding occurs through the movement of extrinsic dislocations along the boundaries. As noted earlier, Rachinger GBS requires accommodation through the movement of intragranular dislocations so that dislocations move into the adjacent grains and pile up at the first obstacle. Two examples of this process are illustrated schematically in Fig. 11. In conventional creep with a large grain size so that $d > \lambda$ as shown in Fig. 11a, the stress concentration at the triple point A leads to intragranular slip in the adjacent grain and these dislocations pile up at the first subgrain boundary at B. By contrast, no subgrains are formed in superplasticity when $d < \lambda$ in Fig. 11b and the stress concentration at the triple point C leads to intragranular slip in the opposing grain and the dislocations then pile up at the opposite grain boundary at D. The rate equations for these two processes are governed by the rate of removal of dislocations from the heads of the pile-ups at B and D.

The stress at the head of a pile-up, σ_p, is given by [81]

$$\sigma_p \approx \frac{2L\tau^2}{G\mathbf{b}} \tag{15}$$

where L is the pile-up length and τ is the magnitude of the shear stress acting on the slip plane in the direction of the Burgers vector. The climb velocity can be introduced for the two separate conditions shown in Fig. 11a and b. In Fig. 11a, the pile-up length of the accommodating dislocations is equal to the subgrain size, λ, where λ varies inversely with stress through Equation 10 and climb occurs intragranularly so that the appropriate diffusion coefficient is D_ℓ; whereas in Fig. 11b, the pile-up length is equal to the grain size, d, and the dislocations climb into the opposing grain boundary so that the appropriate diffusion coefficient is D_{gb}. Using this approach, it has been shown that these mechanisms lead directly to the relationships given by Equations 11 and 14 where A' has a predicted value of ~10 in Equation 11 which is in agreement with a direct experimental measurement of $A' \approx 12$ [73, 82] and A'' in Equation 14 has a predicted value of $\sim 10^2$. It has been demonstrated also that this value of A'' is consistent with the experimental deformation mechanism map shown in Fig. 7 [77].

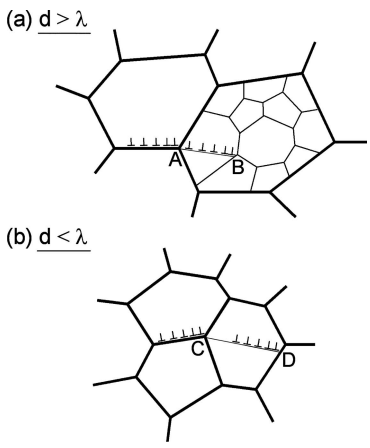

Figure 11 A unified model for Rachinger GBS under (a) conventional creep conditions when $d > \lambda$ and (b) superplastic conditions when $d < \lambda$.

10. The extension of GBS to nanostructured materials

In principle, it seems reasonable to assume that the model developed for Rachinger GBS in superplastic materials, where d < λ, will be equally applicable for even smaller grain sizes down to the nanostructured range where d < 100 nm. In practice, however, there is increasing evidence suggesting the occurrence of new and different mechanisms for GBS in nanostructured solids.

It is reasonable to conclude from Equations 11 and 14 that Rachinger GBS is a diffusion-controlled process and therefore, in agreement with early experimental evidence [83], it is not important in deformation at low temperatures. However, there are recent predictions of the occurrence of low-temperature GBS when using three-dimensional molecular dynamic computer simulations to model the behavior of nanocrystalline solids [84–88]. Furthermore, there is direct evidence for the advent of GBS in electrodeposited Cu having a grain size of only ~28 nm [89]. There is evidence also for the occurrence of GBS in ultrafine-grained materials which were processed using procedures involving the introduction of severe plastic deformation (SPD) as in equal-channel angular pressing or high-pressure torsion [90–92]. A probable explanation for the effect after SPD processing is that the materials contain a very high density of extrinsic dislocations, the grain boundaries are in a non-equilibrium configuration and the extrinsic dislocations permit relatively easy GBS [93]. This proposal is supported indirectly by experimental evidence, obtained using high-resolution electron microscopy, documenting the presence of high dislocation densities adjacent to the grain boundaries after SPD processing [94]. There is also a proposal that the width of the grain boundaries is sufficiently large in nanostructured materials that it is possible to develop macroscopic sliding along planes extending over distances that are much larger than the individual grain size [95, 96]

and there is direct experimental evidence for this type of behavior after SPD processing to produce ultrafine-grain sizes in Cu [97], Ni [97] and Al [98].

Although much of the information on nanostructured and ultrafine-grained materials is in an early stage and not yet fully quantified, there is increasing evidence for the advent of new and additional contributions from GBS in polycrystalline materials when the grain sizes are extremely small. This extension of GBS into the nanostructured range is an exciting new development which will undoubtedly provide stimulating opportunities for further developing the processes and mechanistic aspects of GBS over the next few decades.

11. Summary and conclusions

1. There are two types of grain boundary sliding (GBS): Rachinger GBS which is accommodated by the movement of intragranular dislocations and Lifshitz GBS which accommodates diffusion creep. These two processes produce similar offsets in surface marker lines but Rachinger GBS produces no grain elongation whereas Lifshitz GBS is associated with grain elongation through stress-directed vacancy flow.

2. Procedures are available for measuring the contribution of sliding, ξ, to the total strain during the deformation of polycrystalline materials. These procedures have been used to measure Rachinger GBS in metals, ceramics and geological materials. They have been used also to measure Lifshitz GBS in diffusion creep.

3. Rachinger GBS occurs under two distinct conditions: in conventional creep when the grain size, d, is larger than the equilibrium subgrain size, λ, and in superplasticity when d is smaller than λ. A unified model has been developed to incorporate both types of Rachinger GBS and the resultant rate equations are in excellent agreement with the experimental observations.

4. There is recent evidence, in the form of computer modeling and experimental observations, suggesting an increasing importance of GBS when the grain size is extremely small. However, the precise role of GBS in these nanostructured and ultrafine-grained materials is not fully understood at the present time.

Acknowledgements

This work was supported by the National Science Foundation of the United States under Grant No. DMR-0243331.

References

1. P. PHILLIPS, *Proc. Roy. Soc. London* **19** (1903–1905) 491.
2. E. N. daC ANDRADE, *Proc. R. Soc. A* **84** (1910) 1.
3. *Idem.*, *ibid.* **90** (1914) 329.
4. F. R. N. NABARRO, in "Report of a Conference on Strength of Solids," The Physical Society, London, U.K. (1948) p. 75.
5. C. HERRING, *J. Appl. Phys.* **21** (1950) 437.
6. R. L. COBLE, *ibid.* **34** (1963) 1679.
7. O. A. RUANO, J. WADSWORTH, J. WOLFENSTINE and O. D. SHERBY, *Mater. Sci. Eng. A* **165** (1993) 133.
8. J. WADSWORTH, O. A. RUANO, O. D. SHERBY, in "Creep Behavior of Advanced Materials for the 21st Century," edited by R. S. Mishra, A. K. Mukherjee and K. L. Murty (The Minerals, Metals and Materials Society, Warrendale, PA, 1999) p. 425.
9. G. W. GREENWOOD, in "Creep Behavior of Advanced Materials for the 21st Century," edited by R. S. Mishra, A. K. Mukherjee and K. L. Murty (The Minerals, Metals and Materials Society, Warrendale, PA, 1999) p. 413.
10. K. R. McNEE, G. W. GREENWOOD and H. JONES, *Scripta Mater.* **46** (2002) 437.
11. J. WEERTMAN, *J. Appl. Phys.* **28** (1957) 362.
12. *Idem.*, *ibid.* **28** (1957) 1185.
13. F. A. MOHAMED and T. G. LANGDON, *Acta Metall.* **22** (1974) 779.
14. P. YAVARI and T. G. LANGDON, *ibid.* **30** (1982) 2181.
15. T. ENDO, T. SHIMADA and T. G. LANGDON, *ibid.* **32** (1984) 1991.
16. W. ROSENHAIN and D. EWEN, *J. Inst. Metals* **8** (1912) 149.
17. *Idem.*, *ibid.* **10** (1913) 119.
18. W. ROSENHAIN and J. C. W. HUMFREY, *J. Iron Steel Inst.* **87** (1913) 219.
19. H. F. MOORE, B. B. BETTY and C. W. DOLLINS, *University of Illinois Engineering Experimental Station Bulletin* #272, **32** (1935) 23.
20. *Idem.*, *ibid. 35* (1938) 102.
21. R. KING, R. W. CAHN and B. CHALMERS, *Nature* **161** (1948) 682.
22. F. WEINBERG, *Acta Metall.* **2** (1954) 889.
23. *Idem.*, *Trans. AIME* **212** (1958) 808.
24. J. INTRATER and E. S. MACHLIN, *J. Inst. Metals* **88** (1959–1960) 305.
25. K. E. PUTTICK and R. KING, *J. Inst. Metals* **80** (1951–1952) 537.
26. N. R. ADSIT, and J. O. BRITTAIN, *Trans. AIME* **218** (1960) 765.
27. R. L. BELL and T. G. LANGDON, *J. Mater. Sci.* **2** (1967) 313.
28. R. C. GIFKINS, A. GITTINS, R. L. BELL and T. G. LANGDON, *ibid.* **3** (1968) 306.
29. W. A. RACHINGER, *J. Inst. Metals* **81** (1952–1953) 33.
30. I. M. LIFSHITZ, *Soviet Phys. JETP* **17** (1963) 909.
31. R. L. BELL, C. GRAEME-BARBER and T. G. LANGDON, *Trans. AIME* **239** (1967) 1821.
32. T. G. LANGDON, *Metall. Trans.* **3** (1972) 797.
33. H. BRUNNER and N. J. GRANT, *Trans. AIME* **215** (1959) 48.
34. T. G. LANGDON, *Mater. Sci. Eng. A* **166** (1993) 67.
35. T. G. LANGDON and R. L. BELL, *Trans. AIME* **242** (1968) 2479.
36. J. E. BIRD, A. K. MUKHERJEE and J. E. DORN, in "Quantitative Relation between Properties and Microstructure," edited by D. G. Brandon and A. Rosen (Israel Universities Press, Jerusalem, Israel, 1969) p. 255.
37. T. G. LANGDON, *Phil. Mag.* **22** (1970) 689.
38. R. C. FOLWEILER, *J. Appl. Phys.* **32** (1961) 773.
39. W. L. BARMORE and R. R. VANDERVOORT, *J. Amer. Ceram. Soc.* **48** (1965) 499.
40. D. R. CROPPER and T. G. LANGDON, *Phil. Mag.* **18** (1968) 1181.
41. T. G. LANGDON and J. A. PASK, *Acta Metall.* **18** (1970) 505.
42. T. G. LANGDON, *Scripta Metall.* **4** (1970) 693.

43. W. R. CANNON and T. G. LANGDON, *J. Mater. Sci.* **18** (1983) 1.
44. *Idem.*, *ibid.* **23** (1988) 1.
45. R. S. GORDON, *J. Amer. Ceram. Soc.* **56** (1973) 147.
46. T. G. LANGDON and F. A. MOHAMED, *J. Mater. Sci.* **13** (1978) 473.
47. T. G. LANGDON, *J. Amer. Ceram. Soc.* **55** (1972) 430.
48. *Idem.*, *ibid.* **58** (1975) 92.
49. W. R. CANNON and O. D. SHERBY, *ibid.* **60** (1977) 44.
50. H. C. HEARD and C. B. RALEIGH, *Geol. Soc. Amer. Bull.* **83** (1972) 935.
51. T. G. LANGDON, *Mater. Sci. Eng. A* **283** (2000) 266.
52. J. E. HARRIS, *Metal Sci. J.* **7** (1973) 1.
53. R. C. GIFKINS and T. G. LANGDON, *Scripta Metall.* **4** (1970) 563.
54. I. G. CROSSLAND and J. C. WOOD, *Phil. Mag.* **31** (1975) 1415.
55. E. H. AIGELTINGER and R. C. GIFKINS, *J. Mater. Sci.* **10** (1975) 1889.
56. R. C. GIFKINS, T. G. LANGDON and D. McLEAN, *Metal Sci.* **9** (1975) 141.
57. S. S. SAHAY and G. S. MURTY, *J. Nucl. Mater.* **195** (1992) 320.
58. *Idem.*, *Scripta Mater.* **44** (2001) 841.
59. B.-N. KIM and K. HIRAGA, *ibid.* **42** (2000) 451.
60. T. G. LANGDON, *Metall. Trans. A* **13A** (1982) 689.
61. F. A. MOHAMED, M. M. I. AHMED and T. G. LANGDON, *ibid.* **8A** (1977) 933.
62. P. K. CHAUDHURY and F. A. MOHAMED, *Acta Metall.* **36** (1988) 1099.
63. P. K. CHAUDHURY, V. SIVARAMAKRISHNAN and F. A. MOHAMED, *Metall. Trans. A* **19A** (1988) 2741.
64. S. YAN, J. C. EARTHMAN and F. A. MOHAMED, *Phil. Mag. A* **69** (1994) 1017.
65. A. H. CHOKSHI, A. K. MUKHERJEE and T. G. LANGDON, *Mater. Sci. Eng. R* **10** (1993) 237.
66. T. G. LANGDON, *J. Mater. Sci.* **16** (1981) 2613.
67. R. Z. VALIEV and O. A. KAIBYSHEV, *Acta Metall.* **31** (1983) 2121.
68. T. G. LANGDON, *Mater. Sci. Eng. A* **174** (1994) 225.
69. R. B. VASTAVA and T. G. LANGDON, *Acta Metall.* **27** (1979) 251.
70. P. SHARIAT, R. B. VASTAVA and T. G. LANGDON, *ibid.* **30** (1982) 285.
71. Z.-R. LIN, A. H. CHOKSHI and T. G. LANGDON, *J. Mater. Sci.* **23** (1988) 2712.
72. F. A. MOHAMED and T. G. LANGDON, *Scripta Metall.* **10** (1976) 759.
73. A. BALL and M. M. HUTCHISON, *Metal Sci. J.* **3** (1969) 1.
74. F. A. MOHAMED and T. G. LANGDON, *Acta Metall.* **23** (1975) 117.
75. F. A. MOHAMED, S.-A. SHEI and T. G. LANGDON, *ibid.* **23** (1975) 1443.
76. F. A. MOHAMED and T. G. LANGDON, *Phil. Mag.* **32** (1975) 697.
77. T. G. LANGDON, *Acta Metall. Mater.* **42** (1994) 2437.
78. R. B. VASTAVA and T. G. LANGDON, in "Advances in Materials Technology in the Americas—1980," edited by I. Le May (The American Society of Mechanical Engineers, New York, NY, 1980) vol. 21, p. 61.
79. F. A. MOHAMED and T. G. LANGDON, *Metall. Trans.* **5** (1974) 2339.
80. S. HARPER, in "Structural Processes in Creep" (The Iron and Steel Institute, London, U.K., 1961), p. 56.
81. J. FRIEDEL, Dislocations (Pergamon Press, Oxford, U.K., 1964).
82. P. YAVARI and T. G. LANGDON, *Mater. Sci. Eng.* **57** (1983) 55.
83. R. C. GIFKINS and T. G. LANGDON, *J. Inst. Metals* **93** (1964–1965) 347.
84. H. VAN SWYGENHOVEN and A. CARO, *Appl. Phys. Lett.* **71** (1997) 1652.
85. J. SCHIØTZ, F. D. DI TOLLA and K. W. JACOBSEN, *Nature* **391** (1998) 561.
86. H. VAN SWYGENHOVEN, M. SPACZER, A. CARO and D. FARKAS, *Phys. Rev.* **60** (1999) 22.
87. H. VAN SWYGENHOVEN and P. M. DERLET, *Phys. Rev. B* **64** (2001) 224105.
88. K. S. KUMAR, H. VAN SWYGENHOVEN and S. SURESH, *Acta Mater.* **51** (2003) 5743.
89. L. LU, M. L. SUI and K. LU, *Science* **287** (2000) 1463.
90. R. Z. VALIEV, E. V. KOZLOV, Y. F. IVANOV, J. LIAN, A. A. NAZAROV and B. BAUDELET, *Acta Metall. Mater.* **42** (1994) 2467.
91. R. Z. VALIEV, I. V. ALEXANDROV, Y. T. ZHU and T. C. LOWE, *J. Mater. Res.* **17** (2002) 5.
92. Z. HORITA, K. OHASHI, T. FUJITA, K. KANEKO and T. G. LANGDON, *Adv. Mater.* **17** (2005) 1599.
93. R. Z. VALIEV, *Nature Mater.* **3** (2004) 511.
94. Z. HORITA, D. J. SMITH, M. FURUKAWA, M. NEMOTO, R. Z. VALIEV and T. G. LANGDON, *J. Mater. Res.* **11** (1996) 1880.
95. H. HAHN, P. MONDAL and K. A. PADMANABHAN, *Nanostruct. Mater.* **9** (1997) 603.
96. H. HAHN and K. A. PADMANABHAN, *Phil. Mag. B* **76** (1997) 559.
97. A. VINOGRADOV, S. HASHIMOTO, V. PATLAN and K. KITAGAWA, *Mater. Sci. Eng.* A **319–321** (2001) 802.
98. Y. HUANG and T. G. LANGDON, *ibid.* **358** (2003) 114.